Spanwise structure of wall pressure on a cylinder in axial flow

Arun L. W. Bokde and Richard M. Lueptow
Department of Mechanical Engineering, Northwestern University, Evanston, Illinois 60208

Bruce Abraham
Naval Undersea Warfare Center Division Newport, Newport, Rhode Island 02841

(Received 23 January 1998; accepted 18 September 1998)

The spanwise structure of wall pressure fluctuations was measured in an axisymmetric turbulent boundary layer on a cylinder parallel to the mean flow at a momentum thickness Reynolds number of 2530 and a boundary layer thickness to cylinder radius ratio of 4.81. The measurements were made using miniature hearing aid type condenser microphones with spanwise separations of 0°, 10°, 20°, 30°, 60°, and 90°. An improved wall pressure power spectrum was obtained at low frequencies by utilizing a two-point subtraction method to remove low frequency acoustic background noise of the wind tunnel. The spanwise correlations indicate that the spanwise coherent length of the wall pressure is 30° ($78\nu/u_\tau$ or 0.11δ). The spanwise coherence is weak and concentrated in a frequency band that is substantially lower than the most energetic frequency band of the wall pressure spectrum. A mode number–frequency decomposition of the wall pressure spectrum indicates that the greatest quantity of energy is in the circumferential modes nearest zero. Modes -4 to 4 contain most of the wall pressure energy. Conditional sampling by pressure peak and VITA detection schemes (where VITA was applied to wall pressure to detect strong pressure gradient events) indicate that the spanwise extent of the high pressure peaks and high wall pressure gradients is 60° ($156\nu/u_\tau$ or 0.22δ). [S1070-6631(99)00101-4]

I. INTRODUCTION

Pressure fluctuations at the wall beneath a turbulent boundary layer are the result of the integrated effect of the velocity fluctuations over the wall.[1–3] The wall pressure fluctuations are important in flow induced vibration of structures and acoustical self-noise of structures moving through fluids. Research on wall pressure has centered on planar wall-bounded flows with an emphasis on the wall pressure spectrum and the relationship between the velocity fluctuations in a boundary layer and the wall pressure fluctuations. Often situations of practical importance result in boundary layers on surfaces with significant transverse curvature, such as flow along a long slender cylinder. This particular geometry brings up several unique issues regarding the structure of the turbulent wall pressure. For instance, when the cylinder radius a is small compared to the boundary layer thickness δ, the character of the flow is somewhat wake-like and coherent turbulent structures can pass from one side of the cylinder to the other with relative ease.[4,5] This situation could lead to a strong relationship between the velocity and the wall pressure around the cylinder for which there is no analog with the boundary layer on a flat plate. The cylindrical geometry also suggests a periodicity of the wall pressure around the cylinder with specific mode numbers, the circular analog of spanwise wavenumber. The mode number distribution of the turbulent wall pressure spectrum is of potential importance in certain sonar applications. In this paper, we experimentally investigate the spanwise wall pressure relationship under a turbulent boundary layer on a cylinder in axial flow.

The turbulent boundary layer on a cylinder in axial flow is not significantly different from that on a flat plate when the boundary layer thickness is of the same order or smaller than the radius of the cylinder. For $\delta/a > O(1)$ the transverse curvature of the cylinder begins to alter the characteristics of the flow. The mean velocity profile is fuller and there is an increase in the coefficient of friction.[6] However, the maximum turbulence intensity and VITA detected events in a cylindrical turbulent boundary layer are similar to those of planar wall-bounded flows suggesting that the near wall structure of the boundary layer is similar to that of planar flows with the burst–sweep cycle being the underlying mechanism for the generation of turbulence.[4,5,7] The majority of studies on cylindrical boundary layers have concentrated on the velocity field, while wall pressure measurements have been few. Only Willmarth and Yang,[8] Willmarth *et al.*,[6] and Snarski and Lueptow[7] have made velocity–pressure cross-correlation measurements, and Nepomuceno and Lueptow[9] have made pressure–shear-velocity cross-correlation measurements.

Different spectral bands for the wall pressure correspond to contributions from velocity fluctuations in different regions in the boundary layer based on the use of scaling relationships that lead to the collapse of various regions of the wall pressure spectrum or on wall pressure event or correlation measurements.[7,10–20] Turbulent sources in the inner region ($y^+ < 30$) contribute to the high frequency band of the wall pressure spectrum. (The $+$ superscript denotes nondimensionalization of the distance from the wall y with the friction velocity u_τ and the kinematic viscosity ν.) Through the use of conditional sampling techniques (see Wilczynski *et al.*[21] for a review), large amplitude wall pressure fluctua-

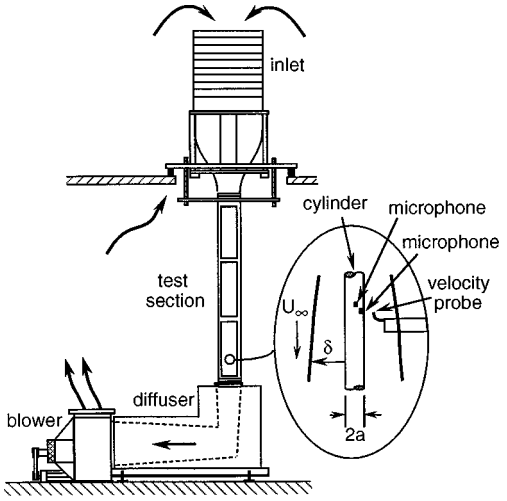

FIG. 1. Sketch of the vertical wind tunnel with a cylinder along its centerline (not to scale). The velocity probe was removed during wall pressure measurements.

tions have been associated with the burst–sweep cycle.[7,9,16,17,22–25]

Turbulent sources in the log region of the boundary layer ($y^+ > 30$ to $y/\delta < 0.6$) contribute to the intermediate frequency range of the wall pressure. The turbulent sources in the outer region of the boundary layer ($y/\delta > 0.6$), including the interface between the boundary layer and the potential region outside the boundary layer, contribute to the low frequency portion of the wall pressure spectrum.[11,14,16,26]

The objective of the investigation described here was to determine the spanwise relationship for the wall pressure beneath a turbulent layer on a long cylinder. This included determination of the average spanwise relationship of the wall pressure based on cross correlation, coherence and circumferential mode decomposition, as well as evaluation of the spanwise relationship of particularly energetic wall pressure events.

II. EXPERIMENTAL SETUP

This investigation was conducted in a low-speed, low-noise open circuit wind tunnel shown in Fig. 1. The wind tunnel test section is vertical to eliminate boundary layer symmetry problems associated with cylinder sag due to gravity. The test section is 3.05 m long with a slightly divergent 0.36 m square cross section resulting in a negligible streamwise pressure gradient. The test section and inlet section are separately supported by a beam system on the second floor to isolate them from floor vibrations and each other. The flexible coupling between the diffuser and fan as well as the 90° bend and acoustical lining of the diffuser reduce the propagation of acoustical noise or vibration from the fan to the test section. The wind tunnel is identical to that used in our earlier research[7,9,27] with the exception that the muffler on the blower outlet was removed after finding that it did not reduce noise contamination in the test section. The turbulence intensity in the test section is less than 0.18% at a free stream velocity of 12 m/s.

The 4.72 m long, 0.953 cm OD cylinder was suspended along the centerline of the test section with its ellipsoidal nose cone 20 cm downstream of the last inlet screen. The nose cone was attached by a wire to a support airfoil located above the last 4 screens of the inlet section. The airfoil was oriented at a right angle to the side of the cylinder containing the wall pressure microphones to minimize any possible effect of turbulence downstream of the support. The cylinder consisted of a 3.35 m long upstream section with an ellipsoidal nose cone which was fabricated from two sections of 0.953 cm OD, 0.16 cm wall acrylic tubing with lengths of brass tubing inside to add rigidity. The 1.37 m long downstream instrumented section was made from 0.953 cm OD, 0.076 cm wall brass seamless tubing that was carefully selected for its straightness and roundness. The joints between the sections were smoothed to assure that the flow was not disrupted. A 1.1 kg weight was attached to the downstream end of the cylinder to keep it in tension. A spring-loaded, foam-lined gripper located 0.5 m downstream from the probes held the cylinder in position and minimized vibration. Visual observation using an 8X telescope showed that the transverse oscillation amplitude was less than 0.003 cm at the 10.6 m/s test velocity inducing a wall pressure due to the vibration that is several orders of magnitude smaller than the wall pressure due to turbulence.

A 1.7 mm high O-ring trip was used 2.10 m upstream of the microphones (0.40 m downstream of the beginning of the test section) to ensure a fully-developed turbulent boundary layer. This distance corresponds to over 1230 trip heights or about 92 boundary layer thicknesses between the trip and the measurement location. The cylinder was centered in the test section by measuring the distances between the cylinder and the duct walls at four axial positions. The alignment with the flow was confirmed based on measuring the wall shear stress using several 0.056 cm OD, 0.015 cm wall, Preston tubes[28,29] positioned around the cylinder just downstream of the microphones. Small Preston tubes have been shown to provide accurate measurements of the wall shear stress on a cylinder based on a flat plate calibration.[6,27] The wall shear stress measured using the Preston tubes varied by less than 2.5% from the mean indicating that the boundary layer was essentially axisymmetric. The streamwise mean velocity profile in the boundary layer measured using a hot wire was slightly fuller than predicted by the cylindrical log law of Lueptow *et al.*,[30] but it was within the expected range of variation. A summary of the experimental and flow conditions are provided in Table I, where U_∞ is the free stream velocity, δ^* and θ are the displacement and momentum thicknesses for a cylindrical boundary layer,[31] and τ_w is the mean wall shear stress. Of particular note is that the curvature ratio is $\delta/a = 4.81$, indicating that the boundary layer is much thicker than the cylinder. Furthermore, $a^+ = a u_\tau/\nu = 148.5$, indicating that about 10 low-speed streaks could be expected around the circumference of the cylinder assuming the usual value of 100 wall units for streak spacing.

The pressure fluctuations on the surface of the cylinder due to the turbulent boundary layer were measured using subminiature electret condenser microphones (Knowles EM-3068). The microphones have a pressure port inner diameter

TABLE I. Experimental and flow conditions.

Experimental conditions	Boundary layer conditions
$\Delta t^+ = 0.744$ (time resolution)	$\delta = 0.0229$ m
$U_\infty = 10.6$ m/s	$\delta/a = 4.81$
$\rho = 1.189$ kg/m^3	$\delta^* = 4.11\times10^{-3}$ m
$\nu = 1.529\times10^{-5}$ m^2/s	$\theta = 3.65\times10^{-3}$ m
$a = 4.76\times10^{-3}$ m	$\mathrm{Re}_\theta = 2530$
$a^+ = 148.5$	$\tau_w = 0.271$ Pa
$d^+ = 22$ (microphone resolution)	$u_\tau = 0.477$ m/s
$d/\delta^* = 0.17$ (microphone resolution)	$u_\tau/U_\infty = 0.045$
	$p_{\mathrm{rms}} = 0.618$ Pa

of 0.70 mm, corresponding to $d^+ = du_\tau/\nu = 22$ for the flow conditions. The microphones were calibrated applying the technique used by Snarski[32] which calibrates both the amplitude and phase of the microphone using a comparison with a reference microphone (Bruel and Kjaer 4134) in a diffuse sound field. The data from the microphones were sampled at 20 kHz after low pass filtering at 10 kHz and high pass filtering at 1 Hz. The microphones were placed at separation angles of $\phi = 10°$, 20°, 30°, 60° and 90° around the circumference of the instrumented section of the cylinder. Not all desired angle combinations could be included on one cylinder, so three different instrumented sections were used. This also acted as a check on the repeatability of the data obtained from different instrumented sections at the same angles.

Although the microphones were small enough to fit inside of the cylinder, it was necessary to separate them between 1.5 mm and 6.8 mm in the streamwise direction due to their size. The angles between microphones and the corresponding spanwise and streamwise separations are given in Table II. In this study we assume that when comparing the response of microphone pairs, the spanwise spacing of the microphones is the primary effect, while the axial spacing of microphones is secondary in importance based on the following arguments. First, Willmarth and coworkers[6,8] found that even for the maximum axial separation in our study, $x = 1.65\delta^*$, the maximum cross-correlation between axially-spaced microphones for $\delta/a = 2$ and 4 was nearly 0.5. Even higher correlations resulted for smaller axial separations. Yet our measurements of the cross-correlation between the microphone spaced axially and circumferentially (shown later in Fig. 3) have maximum cross-correlations that are small fractions of those found by Willmarth for similar separations. Thus, the axial spacing of the microphones makes only a small contribution to the reduced cross-correlation, while the spanwise separation is clearly the dominant factor. Second, Willmarth *et al.*[6] found a significant cross-correlation of 0.15 at an axial separation as large as $x/\delta^* = 8.7$, which is 5 times our maximum axial separation and 25 times our minimum separation. Third, other results for two-point correlations of the wall pressure fluctuations for a DNS investigation of a turbulent boundary layer on a cylinder[33] and wall pressure–streamwise velocity correlations in a turbulent boundary layer on a cylinder[32] indicate a strong cross-correlation in the streamwise direction even for zero lag time. Thus, we assume that the effect spanwise separation between microphones was much more important than the effect of the streamwise separation. Of course, the streamwise separation of microphones required a correction that is based on the convection velocity of structures in the boundary layer, as described later in this paper.

TABLE II. Spanwise and streamwise separation of microphones.

	Spanwise separation		Streamwise separation
ϕ	s^+	$s\delta$	x^+
10°	26	0.036	84
20°	52	0.073	47
30°	78	0.109	131
60°	156	0.218	84
90°	233	0.327	212

III. SPECTRAL AND CORRELATION RESULTS

The power spectral density of the wall pressure was computed with the fast Fourier transform using seven independent time series for each microphone (28.7 s total) providing 560 realizations with 1024 points per realization having a frequency resolution of 19.53 Hz and a random error of 0.042. In the past studies in our lab, the power spectral density was limited to frequencies between 60 Hz and 5228 Hz due to the low frequency acoustic background noise of the wind tunnel and the poor coherence between the condenser microphones in the cylinder and the calibration microphone during the calibration at high frequencies.[7,9] The high frequency cut-off is of little consequence, since there is virtually no energy in the wall pressure at high frequencies. On the other hand, significant low frequency energy is lost by excluding frequencies below 60 Hz. To minimize the effect of the low frequency wind tunnel noise on the wall pressure spectrum, a two measurement point subtraction scheme was used to remove the low frequency noise permitting measurement of the wall pressure spectrum down to 40 Hz. The subtraction scheme utilizes time series from two microphones that are subjected to the same low frequency background noise but are spatially separated so that the turbulent wall pressure is uncorrelated between them.[34] In this case a pair of microphones separated by 90° were used for calculating the spectrum using the subtraction scheme, since signals from this microphone pair had a negligible correlation as shown later in this paper. The corrected power spectrum of the wall pressure is shown in Fig. 2a along with the free stream background noise spectrum. The background noise with the cylinder in place was measured using a Bruel and Kjaer UA 0436 Turbulence Screen with a 1/2 inch Bruel and Kjaer 4134 microphone. This system is specifically designed to measure acoustic noise in a flow environment. The effectiveness of the two-point subtraction scheme in removing acoustic noise from the wall pressure spectrum at low frequencies is evident.

Also plotted in Fig. 2a is the wall pressure spectrum for a planar boundary layer at a similar Reynolds number.[35] There is no significant difference between the flat plate measurements and the cylindrical boundary layer measurements at high frequencies when plotted in the usual inner variables.

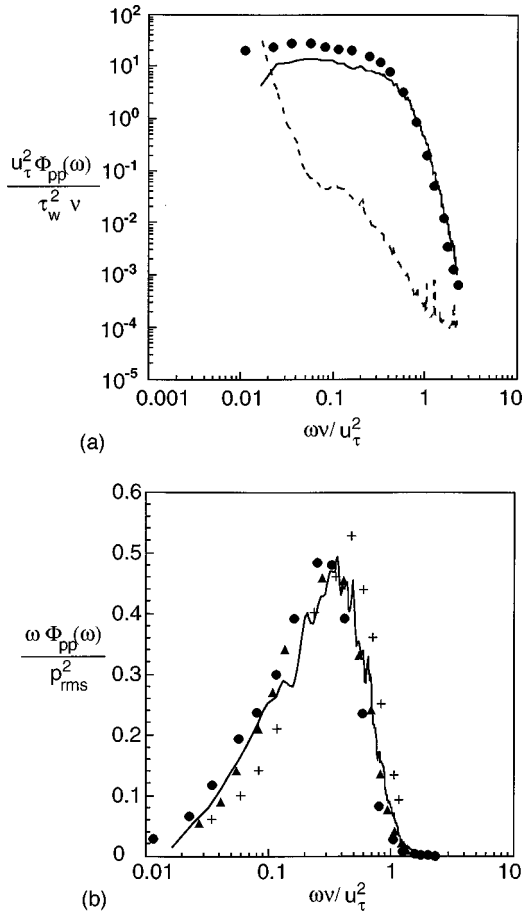

FIG. 2. (a) Power spectra of the wall pressure fluctuations in inner scaling (u_τ, τ_w, and ν). ---, free-stream noise level; —, $\delta/a=4.81$, $\mathrm{Re}_\theta=2530$ (present); ●, flat plate, $\mathrm{Re}_\theta=3386$ (Ref. 35). (b) First moment of the power spectra of the wall pressure fluctuations in inner scaling (u_τ and ν) for cylindrical boundary layers. —, $\delta/a=4.81$, $\mathrm{Re}_\theta=2530$ (present); ▲ $\delta/a=5.04$, $\mathrm{Re}_\theta=2869$ (Ref. 32); +, $\delta/a=5.14$, $\mathrm{Re}_\theta=2220$ (Ref. 9); ●, flat plate, $\mathrm{Re}_\theta=3386$ (Ref. 35).

At low frequencies the differences in the spectra are consistent with previous researchers.[6,8] Since the spectra were obtained at similar Reynolds numbers using microphones of similar size, the difference between the spectra can only be attributed to transverse curvature. A useful form in which to plot power spectra to answer this question is the first moment of the power spectrum $\omega\,\Phi_{pp}(\omega)$ versus log ω, as shown in Fig. 2b, where ω is the angular frequency and $\Phi_{pp}(\omega)$ is the spectral density of the wall pressure. This format provides a visual indication of the relative contribution of a frequency band to the rms wall pressure because equal areas under the curve have equal contributions.[36] The wall pressure spectrum of Snarski and Lueptow[7] and Nepomuceno and Lueptow[9] for the boundary layer on a cylinder are included in Fig. 2b for comparison. The current spectrum compares favorably with the previous measurements on a cylinder. Differences are likely caused by slightly different experimental conditions and experimental error. Willmarth and Yang[8] and Willmarth *et al.*[6] proposed that energy in the wall pressure spectrum for a cylindrical boundary layer is shifted to higher frequencies for $\delta/a=2$ and 4 resulting in lower spectral energy content at low frequencies and higher spectral energy at high frequencies than for a flat plate boundary layer. Based on Fig. 2b, it appears that there may be only a very slight shift in the distribution of spectral energy with frequency due to transverse curvature, at least for small transverse curvature of the order encountered in this study. But differences between the planar and cylindrical wall pressure spectra at low frequencies evident in Fig. 2a may result from the scaling variables, u_τ and δ^*, being different for planar and cylindrical boundary layers. Plotting the data in Fig. 2b using outer scales $\omega\delta^*/U_\infty$ instead of inner scales gives evidence of this. In this case data for the flat plate are shifted to the right so that the data fall below that of the cylinder at low frequencies and slightly above that of the cylinder at high frequencies.

A new result of the experiments presented here compared to the previous measurements in our lab is the expanded range of the spectrum to frequencies below $\omega\nu/u_\tau^2=0.028$. The current results go to a low enough frequency so that the value of the first moment of the spectrum clearly approaches negligible values. With the first moment of the spectra approaching zero at both high and low frequencies, it is evident that all of the spectral energy has been accounted for. Because earlier measurements did not go to as low of a frequency, it was not certain that all of the spectral energy at low frequencies was included.

The temporal cross-correlation between the wall pressure measured at two microphones provides a measure of the temporal relationship between the two signals. The correlation coefficient, $\rho_{ab}(\tau)$, defined as the cross-correlation normalized by the rms value of the two wall pressure signals for a delay time of τ, was calculated using Fourier transform methods. The cross-correlation results were ensemble averaged over 560 realizations consisting of 1024 data points along with 1024 zeros to avoid wrap around aliasing.[37] The data were digitally band pass filtered over frequencies $60<f<5228$ Hz to avoid problems with low frequency noise and poor high frequency calibration coherence. Snarski found that such band pass filtering only slightly altered the pressure–velocity correlations but did not change the character of the correlations.[32]

The auto-correlation and the cross-correlation coefficients at the various spanwise separations are shown in Fig. 3. The correlation peaks are aligned to a delay time of $\tau U_\infty/\delta^*=0$, effectively ignoring the streamwise offset of the measurement microphones. The auto-correlation, labeled 0°, is nearly identical to that obtained by Willmarth *et al.* for $\delta/a=4$.[6] The maximum correlation decreases as the spanwise distance between the pressure probes increases. In addition there is an accompanying small increase in the width of the correlation. The largest angle for which there is a significant correlation is 30°, corresponding to a spanwise separation of $s^+=su_\tau/\nu=78$ and $s/\delta=0.11$, where $s=a\phi$. The correlation between the microphones spaced at 60° is quite small, while at 90° it is negligible. Based on the spanwise cross-correlation between the near wall streamwise velocity and the wall pressure, Snarski[32] found that the velocity was related to the wall pressure peak for angles up to 40°. Thus, the results for the spanwise correlation of the wall pressure in Fig. 3 is consistent with that for the pressure–velocity correlation.

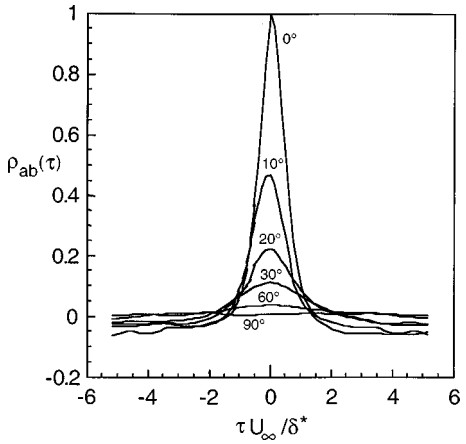

FIG. 3. Temporal cross-correlation of the wall pressure fluctuations for various spanwise angles between the microphones.

Plotting the maximum of the temporal cross-correlation as a function of dimensionless spanwise separation results in the spanwise spatial cross-correlation, $\rho_{ab}(s)$, shown in Fig. 4 along with previous measurements and simulations. The three cylindrical boundary layer cases plotted in Fig. 4 represent a narrow range of curvature ratios based on outer scales ($4.1 \leqslant \delta/a \leqslant 5$), but a wide range of inner scaled radii ($43 \leqslant a^+ \leqslant 1359$) and Reynolds numbers ($414 \leqslant \mathrm{Re}_\theta \leqslant 22{,}300$). Also shown is the cross-correlation for the turbulent boundary layer on a flat plate for comparison. The spanwise correlation drops to zero more quickly for the cylindrical boundary layer than for a flat plate boundary. In all cases, the spanwise correlation approaches zero for a separation angle of about 60°. The similarity between the results of different investigations suggests that an outer scaling is appropriate for the spanwise correlation. Further evidence of this comes from the poor agreement for these cases when the maximum correlation is plotted as a function of the inner-scaled spanwise distance between microphones, s^+, rather than s/δ. When plotted in this way, a stronger correlation results as the radius of the cylinder a^+ increases for similar spanwise separations. An explanation of the scaling of the maximum correlation with outer variables is based on the wall curvature. The curvature of the wall of a cylinder results in a turbulence structure ''touching'' the wall over a limited spanwise extent, since the wall drops away from the structure. The turbulence structures that are large enough to result in significant spanwise correlation are larger structures which scale with the boundary layer thickness. The degree to which the turbulence structure ''touches'' the cylinder is dependent on the ratio of their scales, δ/a. Based on this simple geometric argument, one would expect for a given δ/a the angle over which the turbulence structure ''touches'' the cylinder would be independent of inner scales. Thus, the geometry of the boundary layer transverse curvature, δ/a, governs the spanwise relationship for the wall pressure independent of inner scales.

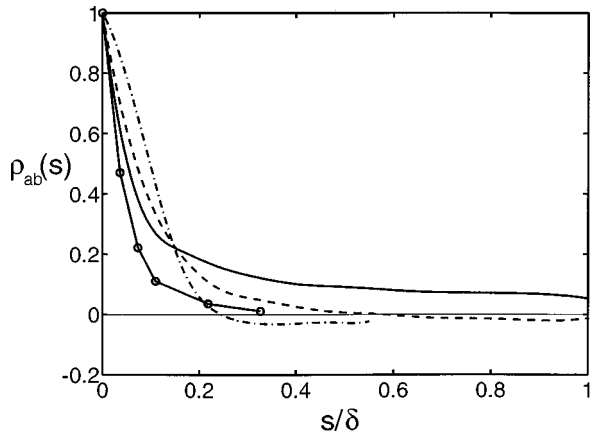

FIG. 4. Spanwise correlation of the wall pressure as a function of dimensionless arclength. ○, $a^+=149$, $\delta/a=4.81$, $\mathrm{Re}_\theta=2530$ (present); -·-, $a^+=43$, $\delta/a=5$, $\mathrm{Re}_\theta=414$ (DNS) (Ref. 33); ---, $a^+=1359$, $\delta/a=4.1$, $\mathrm{Re}_\theta=22\,300$ (experimental) (Ref. 6); —, flat plate, $\mathrm{Re}_\theta=38\,000$ (Ref. 10).

If the geometry of the boundary layer transverse curvature does indeed control the spanwise extent over which the pressure is correlated, then changing δ/a while keeping the Reynolds number the same should result in a variation in the angle for which the pressure is correlated around the cylinder. Indeed, Neves and Moin[33] found that the angle for which spanwise correlation extended around the cylinder increased as δ/a increased for the same momentum thickness Reynolds number. Thus, for a given δ/a, the spanwise correlation extends about the same angle around the cylinder, regardless of Reynolds number. The angle is dependent primarily upon the geometry, δ/a.

The coherence provides a direct indication of the strength of the relationship between two signals as a function of frequency. The degree to which two signals are linearly related in the frequency domain can be determined from the coherence, defined as

$$\gamma_{ab}^2 = \frac{|\Phi_{p_a p_b}|^2}{\Phi_{p_a p_a}\Phi_{p_b p_b}}, \tag{1}$$

where Φ is the single sided spectrum for signals p_a and p_b from microphones a and b. The coherence was computed using fast Fourier transforms after applying a Hanning window to 533 pairs of subrecords of 1024 points each, with a resulting frequency resolution of $\Delta\omega = 123$ rad/s, or $\Delta\omega\nu/u_\tau^2 = 0.00825$, and random error of 0.043. The records were corrected for the time delay resulting from the small streamwise offset of the microphones using the convection velocity as described later for the event detection schemes. The coherence was smoothed using a moving average over a variable number of points. Because of acoustic noise at low frequencies, poor calibration coherence at high frequencies, and the moving average scheme, the results are presented for $0.024 \leqslant \omega\nu/u_\tau^2 \leqslant 1.8$, a slightly narrower frequency range than used for the wall pressure spectra.

The coherence for the microphone pairs at various separation angles is shown in Fig. 5. As expected, the coherence is strongest for the smallest spanwise separation and decreases as the spanwise separation decreases. The greatest spanwise separation for which there is any significant coherence is $\phi = 30°$ ($s^+ = 78$, $s/\delta = 0.11$), the same as the maximum angle for significant correlation in Fig. 3. Since only the large scale pressure structures span the distance between

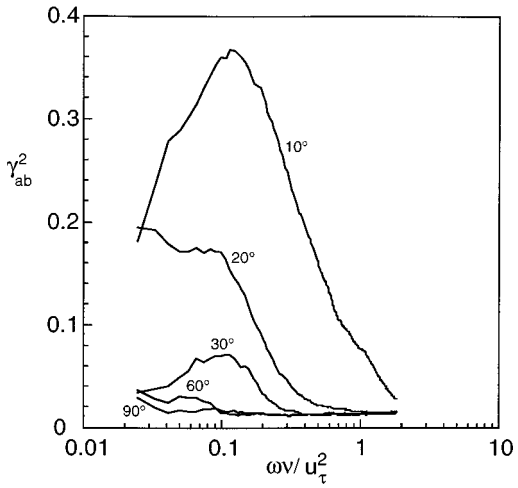

FIG. 5. Coherence of the wall pressure fluctuations for various spanwise angle separations between the microphones.

microphones, the coherence is strongest at lower frequencies. The greatest coherence occurs at frequencies significantly lower than the most energetic frequency band in the spectrum. For instance, at $\phi=10°$ the coherence has a peak at $\omega\nu/u_\tau^2\approx 0.1$, even though the peak in spectral energy occurs at $\omega\nu/u_\tau^2\approx 0.35$. Thus, only a small portion of the spectral energy, that at the lowest frequencies, is felt at both transducers.

The coherence between the pressure and the streamwise velocity measured at $y/\delta=0.095$ and $y/\delta=0.19$ in a similar boundary layer has elevated levels over the frequency band $0.05\leqslant\omega\nu/u_\tau^2\leqslant 0.13$, while either closer to the wall or further from the wall the frequency band with elevated levels is lower.[7] A similar frequency band for elevated pressure–pressure coherence in Fig. 5 suggests that turbulence structures responsible for the relationship in the spanwise pressure are in the same region of the boundary layer and would have a size of about 0.15δ. This scale for the turbulence structures is consistent with the spanwise separation for significant coherence and correlation, $s=0.11\delta$. The pressure–velocity coherence is quite strong for boundary layer-sized structures at a frequency of $\omega\nu/u_\tau^2\approx 0.03$.[7] The pressure–pressure coherence shown in Fig. 5 is not particularly large in this frequency range suggesting that boundary layer–sized structures are not the dominant contributor to the pressure–pressure coherence.

IV. MODE NUMBER DECOMPOSITION OF THE WALL PRESSURE

The flow-induced excitation of cylindrical structures is most easily expressed in terms of the circumferential mode number. The cross-spectrum for the wall pressure measured beneath a flat plate boundary layer at two points with streamwise separation ξ and spanwise separation s, is $\Phi_{PaPb}=\Phi(\xi,s,\omega)$. For this case of a cylindrical boundary layer, the spanwise coordinate in the cross-spectrum is replaced with the arc length, $s=a\phi$, and the streamwise separation is $\xi\approx 0$ resulting in a cross-spectrum $\Phi(\phi,\omega)$ for $-\pi\leqslant\phi\leqslant\pi$. The circumferential mode m component of the wall pressure cross-spectrum is defined as

$$\Phi_m(\omega)=\frac{1}{2\pi}\int_{-\pi}^{\pi}\Phi(\phi,\omega)e^{-im\phi}d\phi. \tag{2}$$

The components of the mode number–frequency spectrum, $\Phi_m(\omega)$, make up the circular analog of the wavenumber–frequency spectrum. However, the cylindrical geometry results in discrete spanwise modes instead of a continuous function of the spanwise wavenumber. Mode 0 corresponds to the circumferentially averaged wall pressure. Modes $+m$ and $-m$ are identical due to symmetry. The wall pressure frequency spectrum at a point, $\Phi(\omega)$, is recoverable as the sum of the spanwise modes,

$$\Phi(\omega)=\sum_{m=-\infty}^{\infty}\Phi_m(\omega), \tag{3}$$

much like the wall pressure frequency spectrum is recoverable from the integration of the wavenumber–frequency spectrum over all wavenumbers in the planar case.

The circumferential components of modes 0 through 4 of the mode number–frequency spectrum were estimated from the circumferential space–time wall pressure cross-correlations as follows. First, the cross-correlation data was linearly interpolated in ϕ. For the interpolation, the cross-correlation was assumed to be zero at $\phi=180°$ based on the negligible cross-correlation measured at $\phi=90°$. The interpolated cross-correlation data were then Fourier transformed to obtain the cross-spectrum as a continuous function of angular separation and frequency, $\Phi(\phi,\omega)$. Finally, the mode number–frequency spectrum was calculated from Eq. (2). Alternatively, it would be possible to begin with the cross-spectrum calculated from the raw data rather than the cross-correlation, but this method was not used because it requires the interpolation of both the real and the imaginary parts of the cross-spectrum in ϕ prior to using Eq. (2) and is more sensitive to the method of interpolation.

The resulting mode 0 through mode ± 4 spectral levels are shown in Fig. 6a. The magnitude of the mode number–frequency spectrum, $\Phi_m(\omega)$, normalized by the frequency spectrum, $\Phi(\omega)$, is plotted as a function of the nondimensional streamwise (convective) wavenumber, $k_c a=\omega a/U_c$, for convenience, where U_c is the convection velocity. The spectral levels decrease with an increasing mode number at a particular convective wavenumber. Except for mode 0, the mode number spectra have a maximum that appears at a higher wavenumber as mode number increases. These results are consistent with the smaller scale structures associated with the higher mode numbers. It is also evident that although the energy in a particular mode decreases with mode number, there is still substantial energy in the higher modes. Nevertheless, much of the energy is included in the modes shown in the figure. The upper solid curve represents the sum of the contributions of modes -4 to 4. Only at higher wavenumbers is there substantial energy in the modes higher

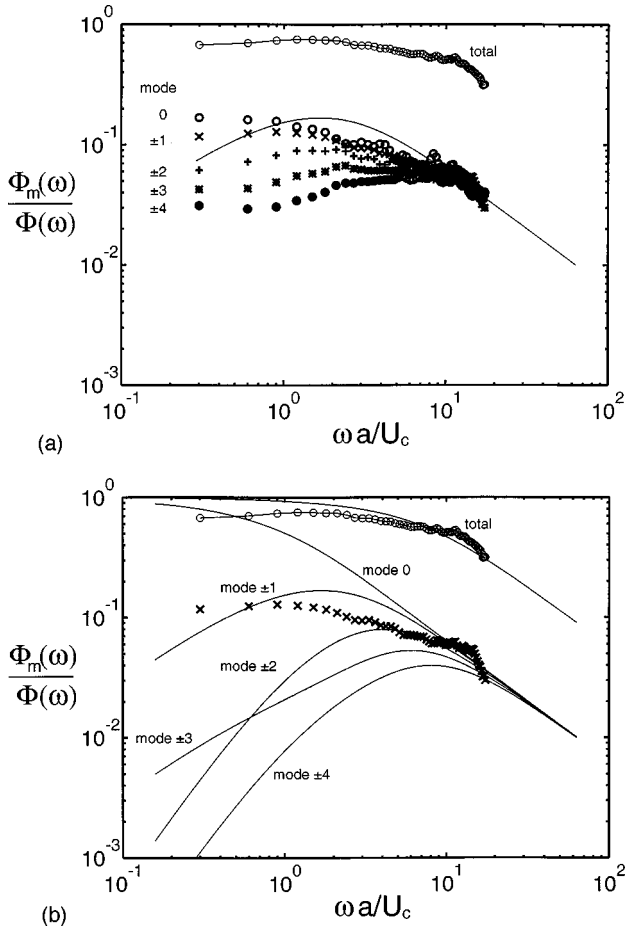

FIG. 6. Mode number decomposition of the wall pressure spectrum. (a) Experimental results for modes 0 to 4: ○, mode 0; ×, modes ±1; +, modes ±2, ∗, modes ±3; ●, modes ±4. The upper solid curve with circles is the sum of modes −4 to 4. The lower solid curve is mode 1 of the model. (b) Model of modes 0 to ±4. The solid curves from top to bottom: sum of modes −4 to 4, mode 0, modes ±1, modes ±2, modes ±3, modes ±4, the upper solid curve with circles is the sum of experimental modes −4 to 4; ×, experimental results for mode ±1.

than those considered. The mode 0 through 4 spectral levels converge for $k_c a > 10$ indicating that all spanwise scales contribute at higher convective wavenumbers.

A simple model of the mode number–frequency spectrum can be based on the Corcos model[38,39] which approximates the wall pressure cross-spectrum, $\Phi(\xi,s,\omega)$, as a product of exponentials. The cross-spectrum decays with increasing streamwise separation, ξ, and spanwise separation, s, while convection occurs in the streamwise direction at a velocity U_c. Replacing the spanwise coordinate in the cross-spectrum model for a flat plate geometry with the arc length, $s = a\phi$, results in

$$\Phi(\xi,\phi,\omega) = \Phi(\omega)[e^{-\alpha|\omega\xi/U_c| - i(\omega\xi/U_c)}][e^{-\beta|\omega(a\phi)/U_c|}], \tag{4}$$

where α and β are the streamwise and spanwise decay constants, respectively. The convection velocity is assumed constant with respect to frequency and spatial separation (ξ or ϕ), although variations in U_c as a function of spatial separation could be accounted for using a numerical analysis.[40]

Evaluating (2) using the cross-spectrum model in (4) using a convective wavenumber, $k_c = \omega/U_c$, results in

$$\Phi_m(k_c) = \Phi(k_c)\,\frac{\beta k_c a[1-(-1)^m e^{-\beta(k_c a)\pi}]}{\pi[(\beta k_c a)^2 + m^2]}. \tag{5}$$

This result is very similar to that obtained when transforming the Corcos model of the wall pressure cross-spectrum into the wavenumber domain using a constant convection velocity for a flat plate, except the exponential term in (5) remains because the field is periodic in the circumferential (spanwise) direction.

The estimated mode m spectrum normalized by the wall pressure frequency spectrum is shown in Fig. 6b using a value of 0.5 for the decay constant β. This decay constant was chosen based on matching the experimental data to the model at high wavenumbers where all modes collapse. Varying the value for β acts to shift the curves horizontally. Using a value of $\beta = 1.3$ results in a better match between the model and the experimental data for the maximum in the spectra for modes 1 to 4, but does not result in the decay at higher wavenumbers matching the experimental results. At very low convective wavenumbers (low frequency), the model predicts the wall pressure to be coherent around the entire circumference of the cylinder and hence the mode 0 pressure asymptotes to the wall pressure spectrum. This is an unrealistic result based on the measured decay in the coherence at large circumferential angles. But the model seems to represent the character of the mode number spectrum for the higher order modes more realistically, especially at higher wavenumbers. Nevertheless, the similarity is only qualitative as is evident by comparing the mode ±1 results for the model to experiments (also shown in Fig. 6b). This is consistent with the failure of the Corcos model to predict the cross-spectrum on a cylinder[8] or in the direct numerical simulation of a planar boundary layer.[41] Nevertheless, the total energy in modes −4 to 4 for the model matches that for the experiment quite well.

V. EVENT DETECTION

Local positive peaks in the wall pressure in a wall-bounded turbulent flow are related to shear layers close to the wall.[7,9,24,42,43] This relationship is bi-directional. That is, when local near-wall shear layers (streamwise accelerations) are detected, sharp positive peaks in wall pressure occur, and vice versa. This bi-directional relationship supports the contention that positive pressure peaks are connected to the local accelerating shear layers associated with the burst cycle.[7,9,22–24,42,43] Negative pressure peak events, which appear with about the same magnitude and frequency as the positive pressure peak events, are not generally associated with a particular turbulence structure near the wall, although they regularly appear in conjunction with positive pressure peak events.[9,21,25]

Typical wall pressure peak events are constructed by detecting instances when the wall pressure exceeds a predetermined level and ensemble averaging such occurrences.[17] A positive event occurs when a wall pressure peak exceeds $kp_{\rm rms}$, where k is usually between 2 and 3, and a negative

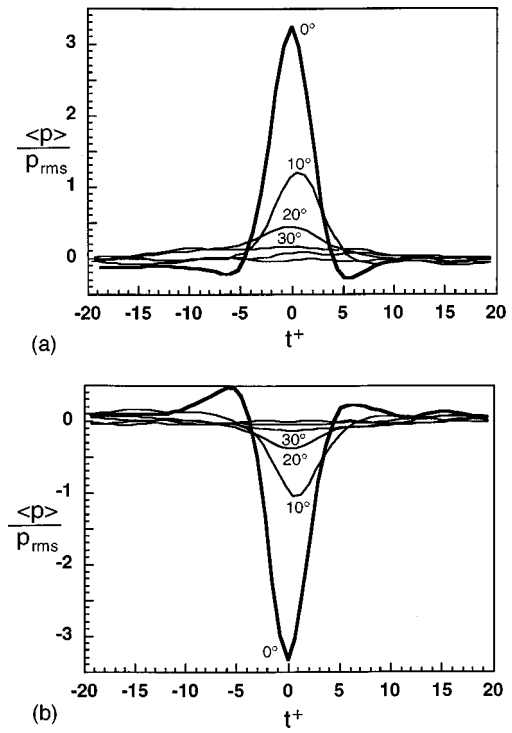

FIG. 7. (a) Conditional average of positive pressure peaks ($k=2.5$) at a spanwise angle of (from largest to smallest at $t^+=0$) $\phi=0°$ (1829 events), $\phi=10°$ (1829 events), $\phi=20°$ (1720 events), $\phi=30°$ (1645 events), $\phi=60°$ (1631 events), $\phi=90°$ (1652 events). (b) The conditional average of negative pressure peaks ($k=2.5$) at a spanwise angle of (from largest to smallest at $t^+=0$) $\phi=0°$ (2031 events), $\phi=10°$ (2031 events), $\phi=20°$ (1958 events), $\phi=30°$ (1815 events), $\phi=60°$ (1782 events), $\phi=90°$ (1798 events).

event occurs when a pressure peak is more negative than $-kp_{\rm rms}$. Here we detect significant wall pressure events at one particular microphone and monitor what is happening simultaneously at other microphones. The ensemble averages of the pressure peaks are shown in Fig. 7 for both positive and negative peak detection where $k=2.5$ and the ensemble averaged event at the detection microphone is the $\phi=0°$ curve. (The brackets $\langle\ \rangle$ represent ensemble averaged quantities.) Other curves represent the ensemble averaged signal at microphones separated from the detection microphone by the specified angle.

The streamwise offset between microphones was taken into account by assuming pure advection of the turbulence field with no distortion at a convection velocity of U_c/U_∞ based on the time shift associated with the maximum cross-correlation amplitude associated with the particular microphone pair. The convection velocity was typically $U_c/U_\infty=0.76\pm0.10$ where the range reflects uncertainty for a given microphone pair. Snarski and Lueptow[7] computed the convection velocity using the pressure–velocity correlations at different streamwise and normal positions to the wall and found similar convection velocities for the velocity probe 85 and 169 viscous units from the wall. Furthermore, the present convection velocity is consistent with the mean convection velocity measured using streamwise separated microphones for cylindrical boundary layers[8] and flat plate boundary layers.[10] Both positive and negative detection wall pressure peaks ($\phi=0°$ in Fig. 7) have time durations of about 10 viscous time units, a magnitude of approximately $\pm3.3p_{\rm rms}$, and small humps of opposite sign before and after the main peak, all of which are consistent with previous experimental results[7,9,17,21,24,42] and DNS channel flow results.[25]

The ensemble averaged pressure signatures at microphones with spanwise separation from the detection microphone are shown in Fig. 7(a) as a function of inner scaled time, $t^+=tu_\tau^2/\nu$, for positive pressure peak events. At $\phi=10°$ ($s^+=26$) from the detection microphone, the magnitude of the pressure peak has decreased by nearly two-thirds to $1.2p_{\rm rms}$ and the peak has broadened slightly. The small humps of opposite sign before and after the main peak disappear at this separation and all greater separations. As the separation angle increases slightly, the magnitude of the peak decreases to $0.4p_{\rm rms}$ at $\phi=20°$ and $0.2p_{\rm rms}$ at $\phi=30°$, and the duration of the peak increases, suggesting spanwise decay of the intensity of the event and smearing in time. At larger separation angles a pressure peak is not evident. The detection schemes detect the strongest peaks, so it can be assumed that the detected peaks are the center of a pressure event. In other words, the detection scheme filters out the other weaker peaks that exist to the side of the center. Thus the spanwise extent to one side from the center of the positive pressure peak is about $\phi=30°$ ($s^+=78$). This leads to a total spanwise extent of the positive wall pressure peak of about $\underline{\phi}=60°$ ($\underline{s}^+=156$, $\underline{s}/\delta=0.22$), where the underbar quantities $\underline{\phi}$ and $\underline{s}$ represent the total spanwise extent of the peak structure.

Results based on detection of negative pressure peaks, shown in Fig. 7b, show the same trend as positive pressure peaks. The magnitude of the pressure peaks adjacent to the detection microphone decrease from $-1.1p_{\rm rms}$ at $\phi=10°$ ($s^+=26$) to $-0.2p_{\rm rms}$ at $\phi=30°$ ($s^+=78$), with a slight broadening of peak with increased separation. At greater spanwise separations, there is no significant pressure signal associated with the detected negative peak. Thus, as with the positive pressure peak, the total spanwise extent of the negative wall pressure peak is about $\underline{\phi}=60°$ ($\underline{s}^+=156$, $\underline{s}/\delta=0.22$).

To check for interference effects of the upstream trigger microphone on the downstream microphone, the peak detection scheme was reversed so that the downstream microphone was the detection microphone. The results are indistinguishable from those shown in Fig. 7. This result has two implications. First, the upstream microphone does not interfere with the wall pressure measured at the downstream microphone. Second, the wall pressure peaks are essentially symmetric from the upstream side to the downstream side about a spanwise line through the wall pressure peak. This result is consistent with the symmetry of ensemble averaged wall pressure peak events in a direct numerical simulation of wall-bounded turbulent flow for a trigger level of $k=3$.[25]

Near wall shear layer (VITA events) have been shown to be associated with positive and negative wall pressure peak events around a cylinder for angles up to 40°,[32] suggesting a total spanwise extent of the velocity structure of about 80°. The spanwise extent for the spanwise pressure–velocity

events are slightly larger, but still consistent with the results for the wall pressure events shown in Fig. 7. For a DNS channel flow, Lueptow[25] found the total spanwise extent of the positive and negative pressure peaks to be $\underline{s}/\delta=0.39$ to 0.56, somewhat larger than the present experimental results. The lack of any peak in the wall pressure at larger separation angles ($\phi=60°$ and 90°) indicates that pressure events are not large enough to extend around the cylinder. Dinkelacker[24] obtained similar results for a turbulent flow in a pipe.

The frequency of occurrence for positive and negative pressure peak events is of the same order of magnitude and the contribution to $p_{\rm rms}$ of both positive and negative excursions of the wall pressure from the mean are nearly the same for this investigation as well as others.[15,17,25,44] This suggests that positive and negative events are equally important. Wilczynski *et al.*[21] suggested that the positive and negative pressure peaks are part of a larger structure, one in which a negative pressure peak is upstream of the positive pressure peak resulting in a local adverse pressure gradient. They detected dual peak events and found that the ensemble averaged event was a composite of a negative peak upstream of the positive peak. Astolfi and Forestier[45] provided further evidence for this by detecting on shear layers close to the wall ($y^+=10$). They found a negative peak upstream of a positive peak of nearly equal magnitude (positive peak followed by a negative peak in time). Using Taylor's frozen field approximation and the relation between the pressure gradient and the spanwise vorticity, a local adverse pressure gradient ($\partial p/\partial x>0$ or $\partial p/\partial t<0$) can be related to an inflectional velocity profile,[9,25] which can be interpreted as a local shear layer in the velocity field. These investigations point to the adverse pressure gradient as being a characteristic wall pressure structure, although Nepomuceno and Lueptow note that a positive pressure peak is always associated with a streamwise velocity acceleration near the wall regardless of how the pressure peak is detected.[9]

Variable Interval Time Averaging (VITA) provides an effective means of detecting local pressure gradients. The VITA detection technique[46] is typically used to detect large gradients in the near-wall streamwise velocity associated with the shear layer of a burst. Applying this technique to pressure fluctuations is unusual, although we have used it successfully to detect wall pressure gradient events.[9,25] An event is said to exist when the short term variance, $\mathrm{var}(t,T)>kp_{\rm rms}^2$, where T is the time over which the short term variance is calculated and k is the threshold level. The number of events detected depend on T and k. Pressure gradient events are further subdivided into negative events ($\partial p/\partial t<0$) corresponding to adverse pressure gradients ($\partial p/\partial x>0$) and positive events ($\partial p/\partial t>0$) corresponding to favorable pressure gradients ($\partial p/\partial x<0$).

Ensemble averaged adverse pressure gradient events are shown in Fig. 8 for $k=1.7$ and $T^+=15$. These values for k and T are based on obtaining a similar number of pressure gradient events as pressure peak events and are similar to those used by Nepomuceno and Lueptow.[9] The ensemble averaged adverse pressure gradient event at the detection microphone ($\phi=0°$) has a larger positive peak amplitude

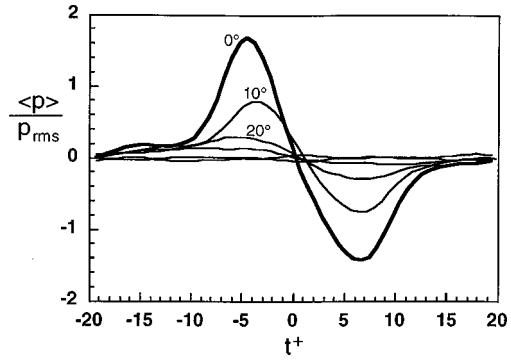

FIG. 8. The conditional average of adverse pressure gradients ($k=2.5$) at a spanwise angle of (from largest to smallest at $t^+=-5$) $\phi=0°$ (1726 events), $\phi=10°$ (1923 events), $\phi=20°$ (1879 events), $\phi=30°$ (1726 events), $\phi=60°$ (1755 events), $\phi=90°$ (1732 events).

($1.7p_{\rm rms}$) than negative peak ($-1.4p_{\rm rms}$). Lueptow[25] and Nepomuceno and Lueptow[47] found the negative peak to be slightly larger in magnitude than the positive peak. The reason for the difference is not clear and not particularly important for this analysis.

At the microphone that is $\phi=10°$ ($s^+=26$) from the detection microphone, the relative magnitudes of the positive and negative peaks are equal to one another and have decreased to $0.7p_{\rm rms}$. The magnitude of the peaks continue to decrease with increasing separation so that by $\phi=30°$, the adverse pressure gradient signature is barely evident. Thus, this separation appears to define the spanwise edge of the structure. The resulting spanwise extent of the adverse pressure gradient is about $\phi=60°$ ($\underline{s}^+=156$ or $\underline{s}/\delta=0.22$), again assuming that the detection signal is at the center of the event. This is the same spanwise extent as was found based on pressure peak detection. In a turbulent channel flow Lueptow[25] found that for an adverse pressure gradient the spanwise extent of $\underline{s}/\delta=0.39$, somewhat larger than the present results for the boundary layer on a cylinder.

VI. CONCLUSIONS

The present investigation succeeded in quantifying the lowest frequency range ($\omega\nu/u_\tau^2\leqslant 0.028$) of the power spectrum of the wall pressure fluctuations through the use of a two-point subtraction scheme. With the better resolution of the low end of the spectrum than has been previously achieved, nearly all of the spectral energy is included in the spectrum. The spanwise correlation and coherence results indicate that the wall pressure is related, on average, about 30° around the cylinder corresponding to $78\nu/u_\tau$ or 0.11δ. Comparing the cross-correlation results to other similar results indicates that the spanwise correlation is best scaled on outer scales. This scaling can be attributed to the degree to which a turbulence structure that scales with the boundary layer thickness ''touches'' the cylinder wall, which is clearly independent of the inner scaling ν/u_τ. As a result, regardless of Reynolds number, turbulent boundary layers with similar ratios δ/a will have similar scaling for the spanwise relationship of the wall pressure around the cylinder, measured in terms of either the angle or the spanwise distance scaled with

an outer scale. The coherence between two microphones separated in the spanwise direction is weak. The peak in coherence is in a frequency band substantially lower than the most energetic frequency band of the power spectrum. The low frequency coherence indicates that the larger eddies of the flow dominate the spanwise coherence.

The decomposition of the wall pressure spectrum into the first five circumferential modes indicates that the mode numbers nearest zero contribute most significantly to the wall pressure spectrum, particularly at low frequencies. At higher frequencies, the contributions for all mode numbers are similar. Most of the spectral energy is recovered in modes -4 to 4. A simple model of the mode number–frequency spectrum based on the Corcos wall pressure spectrum model for a flat plate boundary layer reflects the qualitative character of the experimental mode number–frequency spectrum but fails to match quantitatively at all frequencies.

Particularly energetic events that are isolated from the wall pressure time record using either pressure peak detection or pressure gradient detection are related over a greater distance in the spanwise direction compared to the turbulent field on average. The spanwise extent of these pressure events is 60° (0.22δ) around the cylinder. Thus, these energetic wall pressure structures do not extend around the cylinder but appear randomly around it.

ACKNOWLEDGMENTS

This work was supported by the Naval Undersea Warfare Center Division Newport, Newport, RI, Dr. Marilyn Berliner and Dr. David Hurdis, program managers.

[1]W. W. Willmarth, ''Pressure fluctuations beneath turbulent boundary layers,'' Annu. Rev. Fluid Mech. **7**, 13 (1975).
[2]W. K. Blake, *Mechanics of Flow-Induced Sound and Vibration, Vol. II: Complex Flow-Structure Interactions* (Academic, New York, 1986).
[3]H. Eckelmann, ''A review of knowledge on pressure fluctuations,'' in *Near-Wall Turbulence*: *Proceedings of the 1988 Zoran Zaric Memorial Conference*, edited by S. J. Kline and N. H. Afgan (Hemisphere, New York, 1990), pp. 328–347.
[4]R. M. Lueptow and J. H. Haritonidis, ''The structure of the turbulent boundary layer on a cylinder in axial flow,'' Phys. Fluids **30**, 2993 (1987).
[5]M. K. Bull and W. A. Dekkers, ''Effects of transverse curvature on flow mechanisms in turbulent boundary layers,'' in *Near-Wall Turbulent Flows*, edited by R. M. C. So, C. G. Speziale, and B. E. Launder (Elsevier, New York, 1993), pp. 931–938.
[6]W. W. Willmarth, R. E. Winkel, L. K. Sharma, and T. J. Bogar, ''Axially symmetric turbulent boundary layers on cylinders: mean velocity profiles and wall pressure fluctuations,'' J. Fluid Mech. **76**, 35 (1976).
[7]S. R. Snarski and R. M. Lueptow, ''Wall pressure and coherent structures in a turbulent boundary layer on a cylinder in axial flow,'' J. Fluid Mech. **286**, 137 (1995).
[8]W. W. Willmarth and C. S. Yang, ''Wall-pressure fluctuations beneath turbulent boundary layers on a flat plate and a cylinder,'' J. Fluid Mech. **41**, 47 (1970).
[9]H. G. Nepomuceno and R. M. Lueptow, ''Pressure and shear stress measurements at the wall in a turbulent boundary layer on a cylinder,'' Phys. Fluids **9**, 2732 (1997).
[10]W. W. Willmarth and C. E. Wooldridge, ''Measurements of the fluctuating pressure at the wall beneath a thick turbulent boundary layer,'' J. Fluid Mech. **14**, 187 (1962).
[11]W. W. Willmarth and C. E. Wooldridge, ''Measurements of the correlation between the fluctuating velocities and the fluctuating wall pressure in a thick turbulent boundary layer,'' Report No. AGARD Rep. 456, 1963.
[12]M. K. Bull, ''Wall-pressure fluctuations associated with subsonic turbulent boundary layer flow,'' J. Fluid Mech. **28**, 719 (1967).
[13]W. K. Blake, ''Turbulent boundary-layer wall-pressure fluctuations on smooth and rough walls,'' J. Fluid Mech. **44**, 637 (1970).
[14]R. L. Panton, A. L. Goldman, R. L. Lowery, and M. M. Reischman, ''Low-frequency pressure fluctuations in axisymmetric turbulent boundary layers,'' J. Fluid Mech. **97**, 299 (1980).
[15]G. Schewe, ''On the structure and resolution of wall-pressure fluctuations associated with turbulent boundary-layer flow,'' J. Fluid Mech. **134**, 311 (1983).
[16]Y. Kobashi and M. Ichijo, ''Wall pressure and its relation to turbulence structure of a boundary layer,'' Exp. Fluids **4**, 49 (1986).
[17]A. V. Johansson, J. Her, and J. H. Haritonidis, ''On the generation of high-amplitude wall-pressure peaks in turbulent boundary layers and spots,'' J. Fluid Mech. **175**, 119 (1987).
[18]H. Choi and P. Moin, ''On the space–time characteristics of wall–pressure fluctuations,'' Phys. Fluids A **2**, 1450 (1990).
[19]T. M. Farabee and M. J. Casarella, ''Spectral features of wall pressure fluctuations beneath turbulent boundary layers,'' Phys. Fluids A **3**, 2410 (1991).
[20]W. L. Keith, D. A. Hurdis, and B. M. Abraham, ''A comparison of turbulent boundary layer wall–pressure spectra,'' J. Fluids Eng. **114**, 338 (1992).
[21]V. Wilczynski, M. J. Casarella, and M. Kammeyer, ''A comparison of data on intermittent turbulent and wall pressure events,'' in *Flow Noise Modeling, Measurement, and Control*, ASME Winter Meeting, edited by T. M. Farabee, W. L. Keith, and R. M. Lueptow (ASME, New Orleans, 1993), Vol. NCA 15/FED 168, pp. 25–38.
[22]A. S. W. Thomas and M. K. Bull, ''On the role of wall–pressure fluctuations in deterministic motions in the turbulent boundary layer,'' J. Fluid Mech. **128**, 283 (1983).
[23]J. Kim, ''On the structure of pressure fluctuations in simulated turbulent channel flow,'' J. Fluid Mech. **205**, 421 (1989).
[24]A. Dinkelacker, ''Relations between wall pressure fluctuations and velocity fluctuations in turbulent pipe flow,'' in Ref. 3, pp. 348–360.
[25]R. M. Lueptow, ''Spatio-temporal development of wall pressure events in turbulent wall-bounded flow,'' Eur. J. Mech. B/Fluids **16**, 191 (1997).
[26]P. Bradshaw, ''Irrotational fluctuations near a turbulent boundary layer,'' J. Fluid Mech. **27**, 209 (1967).
[27]A. Wietrzak and R. M. Lueptow, ''Wall shear stress and velocity in a turbulent, axisymmetric boundary layer,'' J. Fluid Mech. **259**, 191 (1994).
[28]J. H. Preston, ''The determination of turbulent skin friction by means of Pitot tubes,'' J. R. Aeronaut. Soc. **58**, 109 (1954).
[29]M. R. Head and V. V. Ram, ''Simplified presentation of Preston tube calibration,'' Aeronaut. Q. **22**, 295 (1971).
[30]R. M. Lueptow, P. Leehey, and T. Stellinger, ''The thick, turbulent boundary layer on a cylinder: Mean and fluctuating velocities,'' Phys. Fluids **28**, 3495 (1985).
[31]H. R. Kelly, ''A note on the laminar boundary layer on a circular cylinder in axial incompressible flow,'' J. Aerosp. Sci. **21**, 634 (1954).
[32]S. R. Snarski, ''Relation between the fluctuating wall pressure and the turbulent structure of a boundary layer on a cylinder in axial flow,'' Report No. NUWC TR 10223, 1993.
[33]J. C. Neves and P. Moin, ''Effects of convex transverse curvature on wall-bounded turbulence. Part 2. The pressure fluctuations,'' J. Fluid Mech. **272**, 383 (1994).
[34]S. P. Gravante, ''Reynolds number effects on time resolved measurements of the wall pressure beneath a turbulent boundary layer,'' MS thesis, Illinois Institute of Technology, 1995.
[35]T. M. Farabee, ''An experimental investigation of wall pressure fluctuations beneath non-equilibrium turbulent flows,'' Report No. DTNSRDC Technical Report 86/047, 1986 (Ref. 19 is an abridged form of this report).
[36]P. Bradshaw, *An Introduction to Turbulence and its Measurement* (Pergamon, New York, 1971), p. 143.
[37]J. S. Bendat and A. G. Piersol, *Random Data: Analysis and Measurement Procedures* (Wiley, New York, 1986).
[38]G. M. Corcos, ''On the resolution of pressure in turbulence,'' J. Acoust. Soc. Am. **35**, 192 (1963).
[39]A. V. Smol'yakov and V. M. Tkachenko, *The Measurement of Turbulent Fluctuations: An Introduction to Hot-Wire Anemometry and Related Transducers* (Springer-Verlag, Berlin, 1983), pp. 147–174.
[40]W. L. Keith and B. M. Abraham, ''Effects of the convection and decay of turbulence on the wall pressure wavenumber–frequency spectrum,'' J. Fluids Eng. **119**, 50 (1997).
[41]B. M. Abraham and W. L. Keith, ''Analysis of the wall pressure field from

a numerical simulation of turbulent channel flow,'' *in Flow Noise Modeling, Measurement, and Control—1995*, edited by R. M. Lueptow, W. L. Keith, and T. M. Farabee (ASME, City, 1995), Vol. NCA–Vol. 19/FED–Vol. 230, pp. 55–65.

[42]J. H. Haritonidis, L. S. Gresko, and K. S. Breuer, ''Wall pressure peaks and waves,'' in Ref. 3, pp. 397–417.

[43]A. V. Johansson, P. H. Alfredsson, and J. Kim, ''Evolution and dynamics of shear-layer structures in near-wall turbulence,'' J. Fluid Mech. **224**, 579 (1991).

[44]C. C. Karangelen, V. Wilczynski, and M. J. Casarella, ''Large amplitude wall pressure events beneath a turbulent boundary layer,'' in *Flow Noise Modeling, Measurement and Control, ASME Winter Meeting*, edited by T. M. Farabee, W. L. Keith, and R. M. Lueptow (ASME, City 1991), Vol. NCA 11/FED 130, pp. 45–53.

[45]J. A. Astolfi and B. E. Forestier, ''Flow noise associated with near-wall turbulence structure,'' in Ref. 44, Vol. NCA 15/FED 168, pp. 1–11.

[46]R. F. Blackwelder and R. E. Kaplan, ''On the wall structure of the turbulent boundary layer,'' J. Fluid Mech. **76**, 89 (1976).

[47]H. G. Nepomuceno and R. M. Lueptow, ''Normal and shear stresses in an axisymmetric turbulent boundary layer on a cylinder,'' in Ref. 41, pp. 119–128.